Interface Mechanical Behavior of Unstabilized Earth Block–Palm Fiber Composites: Experimental and Analytical Pull-Out Analysis

Enzo Candelot-Hours[1], Benjamin Boyer[1], Abdoulatif Diomande[1], Fazia Fouchal[2], Fazilay Abbes[1,2] and Boussad Abbes[2,*]

[1]*University of Reims Champagne-Ardenne, Department of Civil Engineering, UFR SEN, 51100, Reims, France*

[2]*University of Reims Champagne-Ardenne, MATIM, Campus Moulin de la Housse, 51100, Reims, France*

Abstract: The development of sustainable construction materials has renewed interest in bio-based fiber-reinforced earthen composites; however, the mechanical performance of these materials is governed by the fiber–matrix interface, which remains poorly quantified. This study presents an integrated experimental–numerical investigation of the interface behavior between date palm fibers (DPFs) and unstabilized earth blocks.

The experimental program combined tensile testing of DPFs using Digital Image Correlation, compression tests on raw earth, and single-fiber pull-out tests to characterize interfacial behavior from adhesion to frictional sliding. The results show an average Young's modulus of 7.42 GPa for DPFs, 38.09 MPa for raw earth, and an interface stiffness of 487.17 MPa/m. Pull-out tests enabled identification of key interfacial parameters governing load transfer mechanisms.

A numerical model adapted from Gontero's formulation was developed using an equivalent diameter approach to represent the flat geometry of palm fibers while preserving the contact surface. The model successfully reproduces the experimental pull-out response and captures the transition from adhesion to friction-dominated behavior.

This work provides an experimentally calibrated micromechanical framework for predicting the behavior of palm fiber–reinforced earthen composites and contributes to the performance-based design of sustainable bio-reinforced construction materials.

Keywords: Earthen composites, Palm fibers, Pull-out test, Mechanical modeling, Sustainable construction material, Bio-based materials.

1. INTRODUCTION

Earthen construction is gaining renewed interest as a low-carbon and locally available building solution capable of reducing the environmental footprint of the construction sector [1, 2]. Raw earth materials offer recyclability, low embodied energy, and compatibility with circular economy principles. However, their broader adoption remains limited by relatively low tensile strength, brittle failure, and high susceptibility to cracking [3, 4].

To address these limitations, reinforcement strategies have been investigated, particularly the incorporation of natural or waste fibers to enhance ductility and cracking resistance [2, 5, 6].

Natural fibers have shown strong potential for improving the mechanical and durability performance of earthen materials [6,7]. Among them, date palm fibers are abundant agricultural by-products in arid and semi-arid regions and represent a promising reinforcement for sustainable construction [8].

Previous studies have demonstrated the beneficial influence of date palm fibers on the mechanical behavior of rammed earth, gypsum mortar, and compressed earth blocks [9-11]. Improvements in cracking resistance, toughness, and durability have also been reported [12]. Despite these advances, the mechanisms governing load transfer between palm fibers and earthen matrices remain insufficiently understood.

The mechanical performance of fiber-reinforced composites is primarily controlled by the fiber–matrix interface [13]. Efficient stress transfer requires adequate adhesion and frictional resistance, which are commonly characterized through single-fiber pull-out testing [14, 15].

While pull-out methods are widely used in polymer and cementitious composites, their application to earthen materials remains limited. Only recent work has begun exploring the interface behavior of date palm fibers embedded in earth matrices [16]. Consequently, the micromechanical parameters governing adhesion, debonding and sliding are still poorly quantified.

A critical analysis of existing studies highlights several limitations: most research focuses on

*Address correspondence to this author at the University of Reims Champagne-Ardenne, MATIM, Campus Moulin de la Housse, 51100, Reims, France;
E-mail: boussad.abbes@univ-reims.fr

Received on 02-03-2026 Accepted on 01-04-2026 Published on 03-04-2026

E-ISSN: 2311-8717/26

macroscopic mechanical performance rather than micromechanical interface characterization [2, 8], experimental pull-out data for palm fiber–earth systems remain scarce [16], existing modeling approaches were primarily developed for cementitious composites and require adaptation for earthen matrices and flat natural fibers [17, 18]. These gaps limit the development of predictive design tools for bio-reinforced earthen composites.

This study aims to provide an integrated experimental and numerical characterization of the interface between date palm fibers and raw earth by combining: tensile characterization of fibers using Digital Image Correlation [19], mechanical characterization of raw earth, single-fiber pull-out testing, analytical modeling by adapting Gontero's pull-out model to flat natural fibers [17] for future implementation in the finite element software Cast3M [20].

2. MATERIALS AND METHODS

This section presents all the test methodologies, including the various equipment, test benches, and test sample preparation methods used prior to testing.

2.1. Materials

The earthen matrix used in this study originates from the Ksar of Mougheul, a well-known site in the southwest of Algeria, where earthen construction is widely practiced [21]. The material was used in its natural state without chemical stabilization in order to preserve the low environmental impact of the composite and to investigate the intrinsic interaction between earth and plant fibers. Its chemical composition is given in Table **1**.

Table 1: Chemical Composition of Ksar of Mougheul soil [21]

Component	%wt*.
Carbonates (CO3-2)	15.9
Sulphates (SO4-2)	Traces
Chlorides (Cl-2)	0.67
Insoluble (SiO2)	83.43
*%wt: percentage Weight	

The particle size distribution was determined by grain size and sedimentation analyses in a previous study [16], showing that the soil is partly coarse and has a well-graded granulometry.

Prior to specimen preparation, the soil was dried, crushed and sieved to remove coarse particles and ensure repeatable material preparation. The water content used for molding was determined experimentally to obtain adequate workability and compaction. Prismatic specimens were prepared for compressive testing in order to determine the elastic modulus and compressive strength of the raw earth matrix, which are required for the numerical modeling stage. A total of six prismatic samples were tested in compression to ensure statistical representativeness.

Date palm fibers (DPFs) were selected as reinforcement due to their abundance and proven suitability for earthen construction [3, 8-12, 16]. The fibers were manually extracted from palm petioles and cut to the required length for tensile and pull-out testing. Their physical properties and chemical composition are given in Table **2** from a previous study [16]. The fibers analyzed in this study are untreated.

Table 2: Chemical Composition of Date Palm Fibers [16]

Chemical Composition	Value (%)
Cellulose	32 – 35.8
Hemicellulose	24.4 – 28.1
Lignin	26.7 – 28
Fats	7

The mechanical performance of natural fibers is strongly influenced by variability in geometry and microstructure. Therefore, prior to testing, fibers were visually inspected and sorted to minimize defects and ensure representative sampling. A total of six fibers were tested in tension.

2.2. Tensile Characterization of Fibers using Digital Image Correlation

The tensile behavior of date palm fibers was characterized through uniaxial tensile testing combined with Digital Image Correlation (DIC). This optical full-field measurement technique enables non-contact strain evaluation and is particularly suitable for natural fibers exhibiting irregular geometry and heterogeneous deformation fields [9, 22].

A stochastic speckle pattern was applied to the fiber surface to allow displacement tracking during loading. Images were recorded throughout the test and processed using the ARAMIS DIC system [19] to obtain longitudinal strain fields and accurate stress–strain responses.

DIC has become a reference technique for deformation measurement in heterogeneous and bio-based materials due to its ability to capture localized strain concentrations and avoid errors associated with traditional extensometers [22].

According to the recommendations reported in the literature and the ARAMIS system documentation [19], the strain measurement uncertainty is influenced by camera resolution and calibration, subset and step size selection, speckle pattern quality, illumination stability and image noise. Image correlation of the speckle pattern was performed using a facet size of 23 × 23 pixels and a pitch of 17 pixels. Under the adopted acquisition and calibration conditions, the expected strain measurement uncertainty is estimated to be within ±0.15%.

Potential experimental error sources include local fiber heterogeneity and surface roughness, gripping and alignment imperfections. These uncertainty sources are consistent with previous DIC-based characterization of heterogeneous materials [22, 23] and contribute to the scatter observed in the tensile results. Prior to testing, an additional fixture was implemented by placing cardboard plates on either side of the DPF at the gripping jaws (Figure **1**). This interfacial layer acts as a compliant adaptation medium between the specimen and the metallic clamping surfaces.

Figure 1: DPF samples with reinforcement at the gripping zone.

The tensile tests were conducted under displacement-controlled conditions, at crosshead speeds ranging from 0.2 to 0.5 mm/min, in order to ensure quasi-static loading.

Figure **2** illustrates an example of data processing performed using digital image correlation (DIC) software ARAMIS, showing the displacement field at a given stage of the test. During post-processing, a region of interest (ROI) was defined to minimize edge effects and to concentrate the analysis on the central area of the specimen.

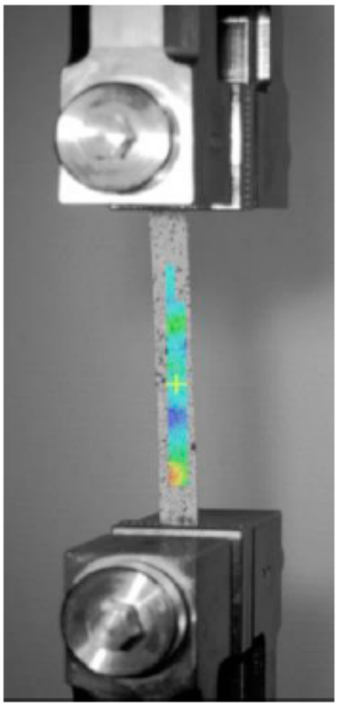

Figure 2: Displacement field obtained by digital image correlation during DPF tensile testing.

2.3. Mechanical Testing of Earth Blocks

The experimental methodology employed for the mechanical characterization of raw earth blocks under compression is based on a specimen preparation procedure and a testing protocol designed to ensure reproducible results. In the absence of standards specifically addressing the mechanical characterization of this material, certain steps of the protocol were defined in accordance with recommendations and practices commonly applied in mortar testing.

The first step in preparing the material involved mixing 70% raw earth with 30% water. The components were combined manually until a homogeneous paste was obtained, ensuring uniform water distribution within the earth matrix. This step is critical to minimize the formation of heterogeneities that could affect the mechanical behavior of the specimens. Once homogenized, the earth paste was placed in a prismatic mold measuring 4×4×16 cm^3, as shown in Figure **3**. The mold was filled in successive layers with manual compaction applied to reduce internal voids and enhance the overall cohesion of the material.

Prior to demolding, the earth blocks felt a natural drying phase in ambient air. This curing step was intended to gradually remove excess water and promote the development of the material's mechanical strength. Drying was conducted under stable outdoor conditions to ensure a gradual reduction in the samples' water content.

Figure 3: Molds containing the prepared raw earth mixture.

Once the blocks had sufficiently dried (after approximately ten days), test specimens for mechanical testing were prepared by cutting the original prisms. The 4×4×16 cm^3 molded blocks were sectioned to produce specimens with a height of 64 mm while retaining a square cross-section of 40×40 mm^2, which decreased to 38×38 mm^2 during drying. This geometry yields specimens suitable for mechanical testing while ensuring adequate stability under loading.

The mechanical properties of the material were evaluated through compression tests performed on these specimens. At the conclusion of the preparation phase, the resulting test specimens were used for compression testing, as illustrated in Figure **4**. Compressive strength was determined from the maximum load recorded during the test, normalized by the cross-sectional area of the specimen.

In addition, the modulus of elasticity was estimated from the initial slope of the stress–strain curve corresponding to the elastic portion of the loading response.

The mechanical tests were performed under controlled loading, with the displacement rate of the compression platen selected to maintain quasi-static conditions. The loading rate was chosen to minimize dynamic effects and to ensure a representative assessment of the material's mechanical behavior, with a value set at 0.5 mm/min.

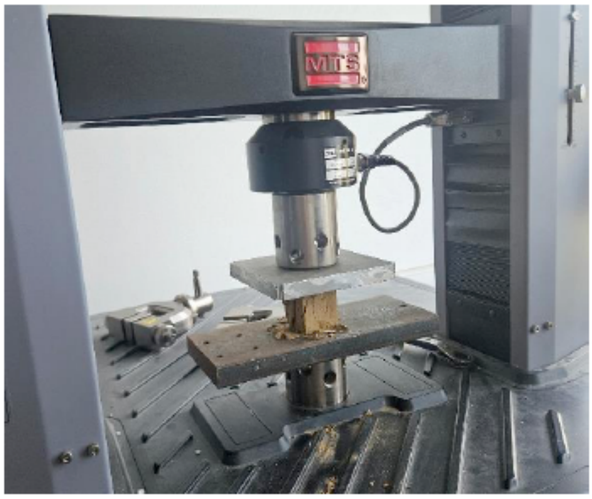

Figure 4: Mechanical characterization of earth blocks under uniaxial compression.

It should be noted that DIC also was evaluated during the compression tests, this was useful for qualitative observation of crack patterns, as illustrated in Figure **5**.

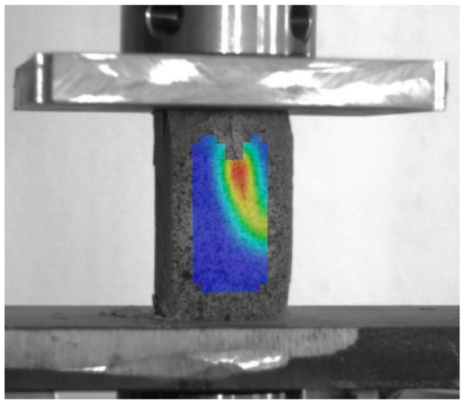

Figure 5: Digital image correlation illustrating crack development during compression testing.

2.4. Pull-Out Test for Interface Characterization

The adhesion between the DPFs and the raw earth matrix was characterized by using pull-out tests. These tests are designed to assess the mechanical behavior of the fiber–matrix interface and to quantify the stress transfer mechanisms developing between the two components.

To limit excessive drying at the fiber–matrix interface and to enhance initial adhesion, the fibers were first immersed in water prior to incorporation into the matrix. This procedure reduces water absorption by the fibers during molding and ensures sufficient moisture at the interface throughout the setting and drying of the raw earth.

Specimens for the pull-out tests were prepared using the same molds employed for the raw earth test specimens described above (Figure **6**). The raw earth matrix was produced following the same protocol, consisting of a mixture of 70% raw earth and 30% water, homogenized until a uniform paste was obtained.

Figure 6: Preparation of specimens for fiber pull-out testing.

With respect to specimen geometry, the fibers used are date palm fibers (DPF), with average dimensions of approximately 0.37 mm in thickness and 7.0 mm in width. During specimen preparation, one end of the fiber was embedded in the raw earth matrix, while the other end remained free to permit the application of tensile load. The embedment length of the fiber within the matrix was 36 mm, and the free length subjected to traction was 80 mm. The raw earth block containing the fiber measured 39 mm in width, 36 mm in height, and 13.2 mm in thickness. This configuration was selected to provide sufficient anchorage for mobilizing interfacial adhesion mechanisms, while enabling controlled fiber extraction and proper placement between the clamping jaws, as illustrated in Figure **7**.

The pull-out tests enabled the measurement of several mechanical parameters characterizing the fiber–matrix interface. Among the analyzed quantities, the maximum pull-out force corresponds to the peak load required to initiate interface failure or fiber slippage. From this maximum force, the average interfacial shear strength between the fiber and the matrix can be estimated. The evolution of fiber displacement was also examined, including the displacement at peak load and the post-peak behavior, which reflects the residual friction between the fiber and the matrix.

Additionally, the energy dissipated during the pull-out process was quantified from the area under the force–displacement curve, providing a measure of the interface's energy dissipation capacity. The initial interfacial stiffness was determined from the slope of the force–displacement curve in the elastic region, a key parameter for calibrating fiber extraction models. Analysis of the post-peak behavior further allowed characterization of the progressive degradation mechanisms of adhesion and friction during fiber extraction and facilitated the calibration of numerical model predictions.

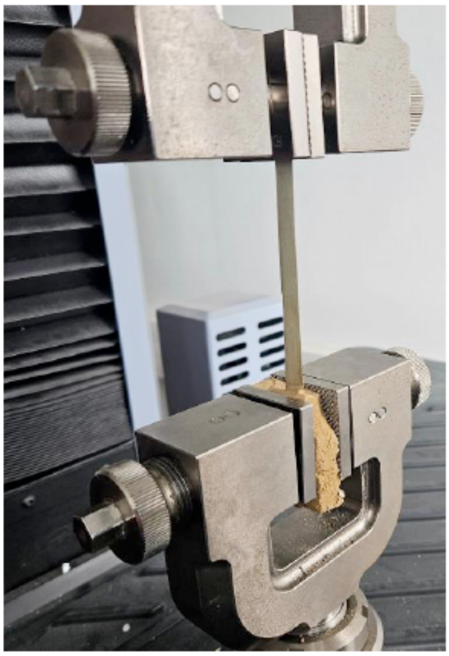

Figure 7: Mechanical characterization of the fiber–matrix interface under pull-out testing.

Some variability was observed among the specimens, likely due to matrix heterogeneity, fiber embedding, or the inherent fragility of the raw earth during loading. These observations underscore the importance of refining the specimen preparation protocol, including molding, compaction, drying, and fiber positioning. Optimizing these steps will improve reproducibility and provide a more representative assessment of the fiber–matrix interface behavior.

A total number of twelve pull-out tests were performed. Natural fiber-reinforced earthen materials exhibit inherent variability due to several factors [13, 16], such as natural variability of fiber geometry and microstructure, heterogeneity of the earthen matrix, variability in fiber surface roughness, slight differences in embedment and specimen preparation.

These factors explain the scatter observed in the experimental results and are consistent with previous studies on plant fiber composites [14-16].

2.5. Pull-out Test Modeling

As part of the investigation of the mechanical behavior of the interface between raw earth and DPF, the model proposed by Gontero [17] was selected as the basis for numerical simulations. Originally developed to describe the behavior of fiber-reinforced concrete, this model is implemented in the Cast3M finite element software and coded in Fortran 90. It provides a suitable theoretical framework for analyzing the mechanical response of fiber-reinforced composite materials.

The model proposed by Gontero [17] was specifically developed to simulate the mechanical behavior of fiber-reinforced concrete and is designed to complement and extend the Fluendo3D orthotropic cracking model [18]. Its primary objective is to provide a more realistic representation of the influence of fibers on the material's mechanical response, particularly with respect to damage evolution and crack propagation.

This model is particularly suitable for the present study because it describes the full pull-out curve, accounts for progressive debonding, incorporates frictional sliding after debonding and can be implemented in finite element simulations.

The initial equations for the extraction of a fiber anchored at one end are based on the works of Nammur *et al*. [24], Zhan and Meschke [25, 26], and Rajagopalan and Parameswaran [27], who proposed realistic models for fiber pull-out.

Selecting an appropriate model is a critical step for ensuring the relevance of numerical simulations when analyzing the mechanical behavior of composite materials. Gontero's model describes fiber extraction from a matrix and introduces a constitutive law for post-peak behavior, accounting for the influence of fiber inclination within the matrix. In this study, the focus is limited to the characterization of straight date palm fibers embedded in a raw earth matrix. The following section summarizes the equations of Gontero's model for straight fiber extraction. Fiber extraction is governed by three main phases, beginning with an initial interface elasticity phase, which is linear and occurs within the range of reversible deformation. The elastic behavior of the interface can be expressed by the following equation:

$$\tau_e(x) = H_f . s_e(x) \quad (1)$$

This represents the evolution of the shear stress $\tau_e(x)$ at the interface between the fiber and the matrix, and the stiffness modulus H_f of the interface will, for example, be defined during this phase and determined by analyzing the results of experimental pull-out tests, taking into account the relative slip $s_e(x)$.

The modeling is based on Hooke's law, yielding a differential equation that describes the distribution of stress F_e along the fiber on the elastic phase:

$$\frac{d^2F_e}{dx^2} - k_c^2 . F_e = 0 \quad (2)$$

with the characteristic parameter k_c, which combines geometric and material properties such as:

$$k_c = \sqrt{\frac{4.H_f}{E_f.\phi_f}} \quad (3)$$

where H_f represents the interface stiffness, E_f the elastic modulus of the fiber, and ϕ_f its diameter. It should be noted that in our case we are dealing with a flat fiber, therefore an equivalent diameter will be determined that ensures the same contact surface area between the DPF and the raw earth matrix.

The boundary conditions of the problem are defined by the force applied at $x = 0$ and the absence of stress at the anchored end $x = L$:

$$F_e(0) = F_m \text{ and } F_e(L) = 0 \quad (4)$$

Solving the differential equation leads to the distribution law of the normal force along the fiber:

$$F_e(x) = \frac{F_m.e^{k_c.x}.(e^{2.k_c.(L-x)}-1)}{e^{2.k_c.L}-1} \quad (5)$$

2.5.1. Influence of Interface Stiffness

The force profile depends on the interface stiffness H_f. If H_f is high, the force decreases very quickly, whereas if it is low, the interface is sheared more uniformly over the length. From the force distribution, we can deduce the shear stress profile at the interface $\tau_e(x)$ and the associated slip $s_e(x)$.

$$\tau_e(x) = \frac{1}{\pi.\phi_f} . \frac{dF_e(x)}{dx} \quad (6)$$

$$\tau_e(x) = -\frac{F_m.k_c.(e^{k_c.(2L-x)}+e^{k_c.x})}{\pi.\phi_f.(e^{2.k_c.L}-1)} \quad (7)$$

$$s_e(x) = -\frac{\tau_e(x)}{H_f} = \frac{F_m.k_c.(e^{k_c.(2L-x)}+e^{k_c.x})}{\pi.\phi_f.H_f(e^{2.k_c.L}-1)} \quad (8)$$

These equations describe the behavior during the elastic phase of the interface.

The elastic phase is followed by a fiber debonding phase, initiated when the interfacial shear stress exceeds the maximum shear strength of the interface. An interfacial crack subsequently propagates over a length L_d . This debonding corresponds to the progressive loss of chemical adhesion, which is replaced by frictional interaction, modeled through an interfacial shear stress τ_d. During the fiber debonding phase, the total tensile force F_m applied to the fiber is expressed as the sum of the contributions from the still-bonded region (F_c) and the debonded region (F_d):

$$F_m(L_d) = F_c(L_d) + F_d(L_d) \tag{9}$$

The frictional force F_d is proportional to the debonded length, while the residual force F_c is determined by considering the maximum interfacial shear stress $\tau_{\max}$ at the crack front, with the initial embedment length L replaced by the remaining bonded length $(L - L_d)$:

$$F_d = \pi.\phi_f.\tau_d.L_d \tag{10}$$

$$F_c = \frac{\tau_{max}.\pi.\phi_f.(e^{2.k_c.L} - e^{2.k_c.L_d})}{k_c.(e^{2.k_c.L} + e^{2.k_c.L_d})} \tag{11}$$

The total slip of the fiber, s_m, is defined as the sum of the critical slip at the debonding front (s_{crit}) and the accumulated slip within the frictional zone (s_d). The critical slip is given by $s_{\text{crit}} = \tau_{\max}/H_f$. The slip in the debonded region is obtained by integrating the elastic constitutive relation:

$$s_m = s_{crit} + s_d \tag{12}$$

$$s_d = \frac{\pi.\phi_f}{E_f.A_f}.\left(\tau_d.L_d^2 + \frac{\tau_{max}.(e^{2.k_c.L} - e^{2.k_c.L_d})}{k_c.(e^{2.k_c.L} + e^{2.k_c.L_d})}\right) \tag{13}$$

When debonding becomes unstable, the fiber enters the pull-out phase. This stage is governed by a constitutive law that characterizes the frictional interaction between the fiber and the matrix. The model assumes uniform slip along the embedded length and neglects elastic recovery relative to the magnitude of the pull-out displacement.

The evolution of the interfacial shear stress during extraction, denoted τ_p, is complex and arises from the combined effects of matrix abrasion, particle accumulation, and end-defect mechanisms. These considerations lead to the formulation of a phenomenological relationship expressing τ_p as a function of the pull-out slip s_p:

$$\tau_p(s_p) = \underbrace{\tau_d.\frac{s_k}{s_k + s_p}}_{Marix\ abrasion} + \overbrace{M_0.\frac{s_p.L}{(L+L_0)^2}}^{Particle\ accumulation} + \underbrace{\frac{f_0}{\pi.\phi_f.(L - s_p)}}_{\text{end−defect mechanisms}} \tag{14}$$

where s_k drives the abrasion kinetics, M_0 is the particle-related work hardening modulus, and L_0 is a characteristic length weighting the impact of the anchorage length.

The overall force F_m required for extraction (Figure **8**) is deduced from the average stress acting on the residual contact surface. By integrating the previous relationship, we obtain the total force:

$$F_m(s_p) = \pi.\phi_f.(L - s_p).\tau_p(s_p) \tag{15}$$

The term f_0 represents the force required to mobilize the end defect within the fiber channel. The transition from the debonding phase to the pull-out phase induces an instability, whereby the stored elastic energy is abruptly released, resulting in a kinematic jump associated with the activation of the end defect. This mechanism requires an initial slip $s_0 = f_0/k_0$ for activation.

The total fiber slip, s_m, is thus defined as the sum of all accumulated kinematic contributions:

$$s_m = s_{crit} + s_d + s_0 + s_p \tag{16}$$

where s_{crit} denotes the critical elastic slip, s_d the slip within the debonded zone, s_0 the slip associated with end-defect mobilization, and s_p the pure pull-out slip.

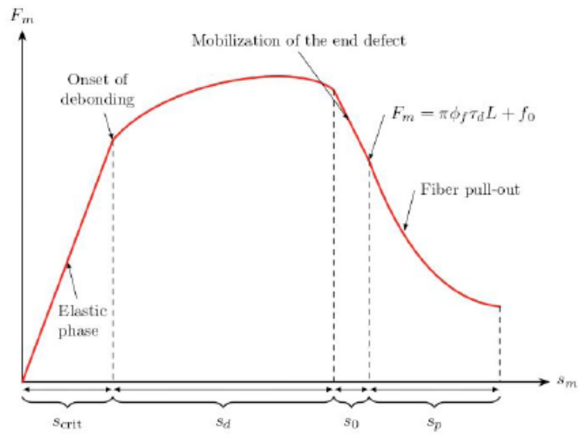

Figure 8: Total force-displacement curve.

2.5.2. Model Assumptions and Limitations of the Approach

The adapted pull-out model is based on a set of simplifying assumptions commonly adopted in micromechanical analyses of fiber-reinforced composites. Both the earthen matrix and the palm fiber are assumed to behave as linear elastic materials within the investigated loading range. Interfacial stresses are considered uniformly distributed along the embedded length, and debonding is assumed to initiate when a critical interfacial shear stress is reached. After complete debonding, the interface response is governed by Coulomb-type friction, which controls the sliding stage of the pull-out process. Thermal and moisture effects are neglected in the present formulation in order to focus on the mechanical aspects of the interface behavior under monotonic loading.

Despite its ability to reproduce the main features of the pull-out response, the proposed framework involves several limitations. The equivalent diameter approach simplifies the real ribbon-like geometry of palm fibers and therefore neglects local stress concentrations and anisotropic contact conditions at the interface. In addition, the model assumes uniform interfacial properties, whereas natural fibers and earthen matrices inherently exhibit significant heterogeneity. Time-dependent effects such as creep, shrinkage, and moisture interactions are not considered, and the influence of fiber surface roughness is represented indirectly through friction parameters. Consequently, the model should be interpreted as a simplified yet physically meaningful representation of the dominant mechanisms governing fiber pull-out.

2.5.3. Parametric Study

This section presents a detailed parametric study of the model employed in this work. The objective is to quantify and characterize the influence of the model parameters on the predicted response. Through a systematic variation of each parameter, the analysis identifies the most influential factors, evaluates the sensitivity of the model, and enhances the understanding of the overall system behavior. The results provide a consistent framework for interpreting model performance and for guiding subsequent calibration and optimization.

Figures **9** to **13** present the influence of key model parameters, namely interface stiffness, interfacial shear strength, characteristic slip, fiber length, and equivalent fiber diameter.

Influence of interfacial shear strength

An increase in the interfacial shear strength primarily affects the initial portion of the pull-out curve by delaying the onset of debonding. Higher adhesion improves the efficiency of stress transfer between the matrix and the fiber, leading to an increase in the peak pull-out force. From a micromechanical perspective, stronger adhesion requires higher shear stresses to initiate interfacial damage, thereby increasing the elastic energy stored in the system before debonding begins. This mechanism is directly related to the crack-bridging capability of fibers, as stronger adhesion enables fibers to sustain higher loads prior to interfacial failure.

Influence of frictional stress

Frictional stress governs the post-debonding stage and therefore controls the residual load during fiber sliding. Increasing the friction coefficient results in a higher plateau in the pull-out curve and a significant increase in the energy dissipated during extraction. Physically, this behavior reflects the role of surface roughness and mechanical interlocking between the fiber and the earthen matrix. A higher frictional resistance enhances energy dissipation and contributes to improved toughness and post-cracking ductility of the composite.

Influence of embedded length

The embedded length has a major influence on both peak load and pull-out energy. Longer embedded lengths increase the contact surface between the fiber and the matrix, allowing greater interfacial stresses to develop. As a result, both the maximum pull-out force and the sliding energy increase. This behavior highlights the importance of fiber anchorage in crack-bridging mechanisms: longer fibers can transfer stresses over larger distances, improving resistance to crack propagation.

Influence of fiber stiffness

The fiber elastic modulus influences the slope of the initial portion of the pull-out curve. Stiffer fibers deform less under load, allowing faster transfer of stresses to the interface and resulting in a steeper initial response. This parameter therefore governs the stiffness of the crack-bridging mechanism and the ability of fibers to limit crack opening.

Implications for composite behavior

Overall, the parametric study confirms that the pull-out response results from a balance between adhesion-controlled load transfer and friction-controlled energy dissipation. Adhesion governs the load-bearing capacity, while friction governs toughness and ductility. This balance is essential for optimizing the mechanical performance of palm fiber–reinforced earthen composites and provides guidelines for tailoring fiber treatment, geometry, and embedment conditions to achieve improved structural performance.

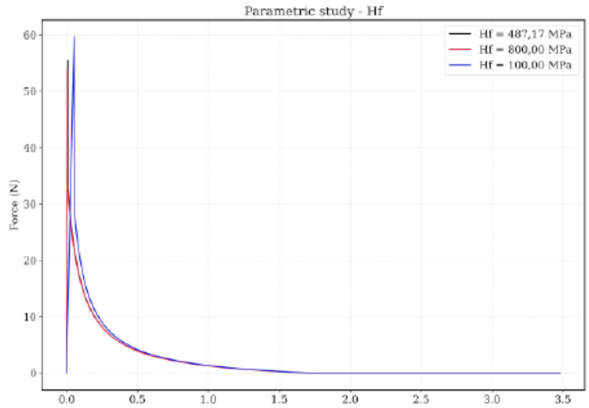

Figure 9: Influence of interace stiffness.

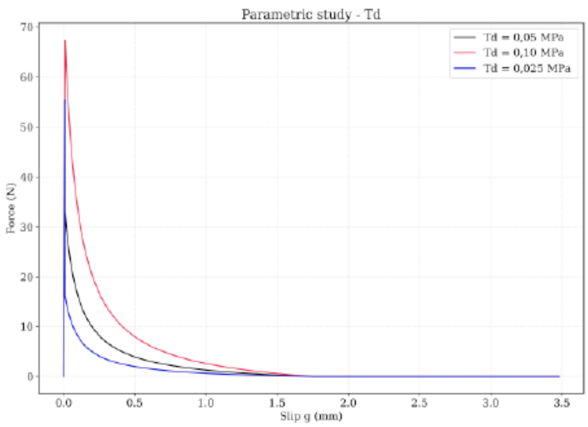

Figure 10: Influence of interfacial shear stress τ_d.

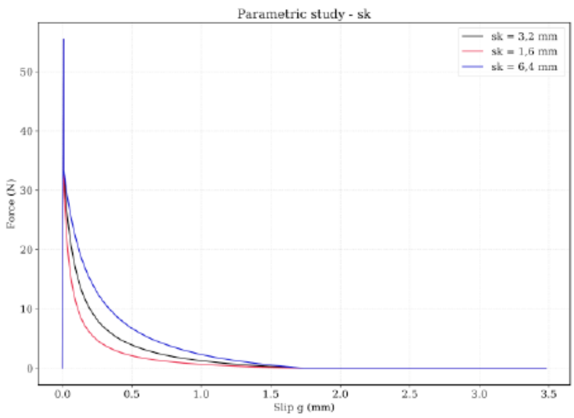

Figure 11: Influence of characteristic slip.

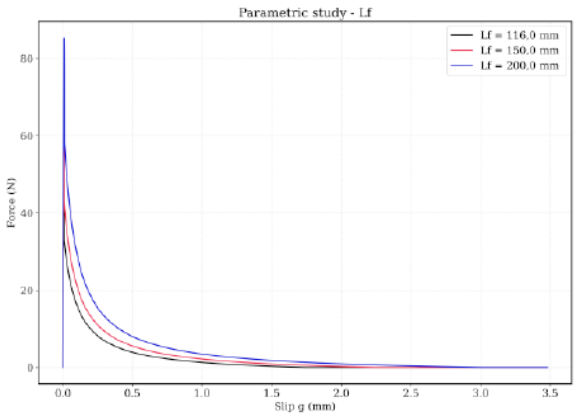

Figure 12: Influence of fiber length.

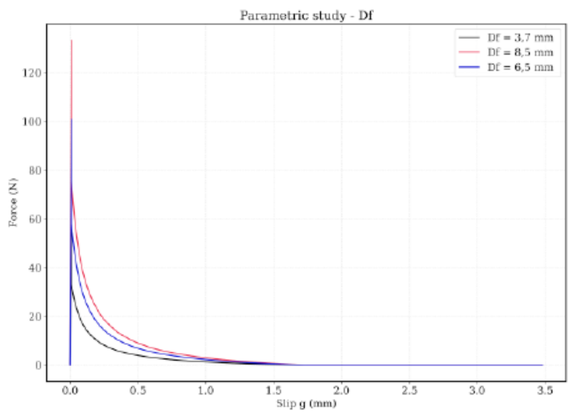

Figure 13: Influence of fiber equivalent diameter.

3. RESULTS AND DISCUSSION

This section presents the experimental results obtained from all tests conducted in this study. The objective of this phase is to characterize the mechanical behavior of date palm fibers, both individually and in combination with raw earth, in order to inform the numerical model described above. The experimental results are subsequently compared with the numerical predictions to assess the validity and performance of the model in simulating the fiber–matrix behavior under pull-out conditions.

3.1. Mechanical Performance of DPF

This section presents the experimental characterization of DPFs. Figure **14** shows the stress–strain response obtained from digital image correlation and tensile testing. The fibers exhibit brittle, quasi-linear elastic behavior up to sudden rupture, with no significant plasticity, validating the assumption of linear elasticity. The slopes of the linear regions were used to determine the longitudinal Young's modulus, which shows some variability typical of natural lignocellulosic materials.

Failure mode analysis (Figure **15**) indicates that fiber width does not influence fracture behavior. Fibers consistently fail in a stepwise manner, with microfibrils fracturing sequentially rather than simultaneously.

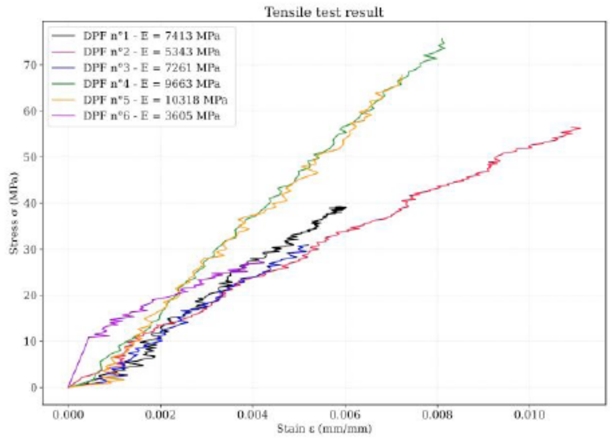

Figure 14: Stress–strain response of DPF under tensile loading.

The average Young's modulus E was 7267 MPa, which will be used to calculate the characteristic interfacial parameter k_c. The fibers exhibited an average maximum stress σ_{max} of 49.54 MPa and an ultimate strain ε_{fu} of 6.7‰. These values are consistent with those reported in the literature, such as by Mahi *et al*. [16].

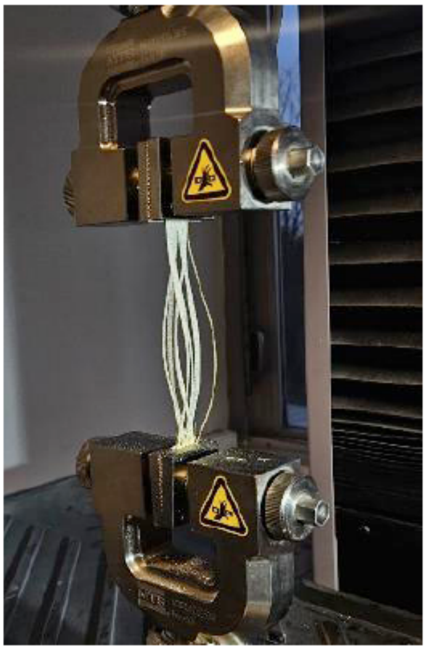

Figure 15: DPF failure mode.

3.2. Mechanical Performance of Earth Blocks

This section presents the experimental results of the compressive characterization of raw earth. The results are illustrated in Figure **16**, which shows the stress–strain behavior of all tested specimens, based on the recorded load and deformation data obtained from the testing machine.

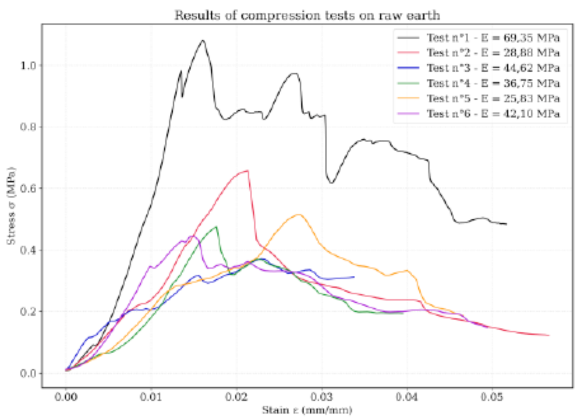

Figure 16: Stress–strain response of raw earth under compression tests.

The specimens initially exhibited an elastic response, followed by a quasi-brittle failure characterized by strain softening. The stress–strain relationship was approximately linear at the onset of loading, enabling the determination of the Young's modulus for each sample. The results reveal significant variability in both Young's modulus (ranging from 25.83 to 69.35 MPa) and peak stress (ranging from 0.34 to 1.08 MPa), reflecting the inherent heterogeneity of raw earth as a natural material.

Instead of a sudden, complete failure, a stepwise stress drop was observed, indicating progressive damage. This behavior is associated with the gradual development of microcracks, allowing the specimen to retain partial load-bearing capacity prior to final collapse.

An average Young's modulus of approximately 38.09 MPa was determined. The analysis of compressive strength (σ_{max}) reveals significant variability, highlighting the sensitivity of the material. This variability is likely influenced by slight differences in specimen preparation, such as local moisture content, degree of compaction, and the presence of macropores.

Nevertheless, the overall mechanical response, particularly the stepwise stress drops observed during the softening phase, is consistent with behaviors reported in the literature for geomaterials and raw earth masonry [28, 29].

3.3. Pull-Out Behavior

This section presents the results of the pull-out test conducted to characterize the mechanical behavior of the fiber–matrix interface. A representative curve is shown in Figure **17**, illustrating the evolution of the pull-out force as a function of fiber slip.

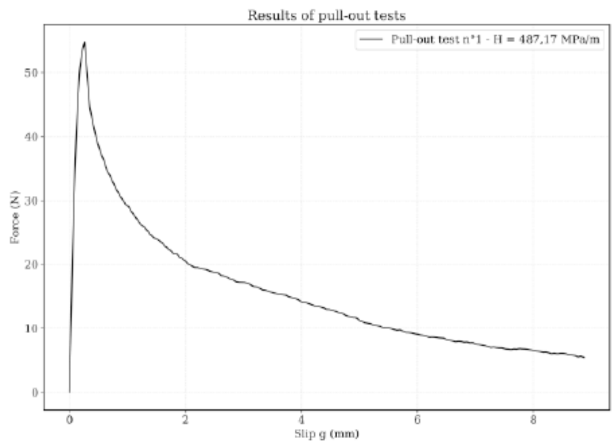

Figure 17: Evolution of the extraction force of the DPF.

This curve clearly identifies the characteristic phases of fiber–matrix interfacial behavior. The analysis reveals the following stages:

- Pre-peak adhesion phase: The initial loading stage is characterized by a rapid and nearly linear increase in force with minimal slip. This elastic regime reflects the combined effects of chemical adhesion and initial mechanical anchorage between the fiber and the matrix. The slope of this linear portion was used to determine the interfacial stiffness, evaluated at MPa/m, a key parameter for the application of Gontero's model [12].

- Bond strength and debonding: The force subsequently reaches a maximum value of approximately 55 N, corresponding to the interfacial bond strength. This peak marks the onset of interfacial damage, initiating the debonding process as the chemical adhesion is progressively lost.

- Frictional slip phase: Following complete debonding, the response enters a post-peak softening regime. The residual pull-out force is then governed by frictional interactions between the fiber surface and the surrounding matrix. The force decreases nonlinearly with increasing slip, reflecting the reduction in effective contact area and the progressive extraction of the date palm fiber.

In the case of an untreated date palm fiber (DPF) embedded in unstabilized raw earth, the influence of the intrinsic mechanical properties of the fiber appears to be relatively limited. Parameters such as the Young's modulus or elastic strength of the fiber have only a minor effect on the overall response observed during the pull-out test.

This behavior can be primarily attributed to the governing failure mechanism. In most configurations, degradation occurs preferentially at the fiber–matrix interface, before the fiber itself reaches its mechanical limit. Consequently, the load-bearing capacity of the system is predominantly controlled by interfacial properties, including interfacial shear strength and frictional mechanisms mobilized during progressive fiber slip.

Thus, within the investigated context, the pull-out response is governed more by adhesion and friction at the interface than by the intrinsic mechanical properties of the fiber. This finding underscores the importance of characterizing and modeling interfacial phenomena to reliably describe the interaction between DPFs and the raw earth matrix.

3.3. Model–Experiment Comparison

This section presents a comparison between the experimental results and the calibrated numerical model response. It is devoted to the validation of the interfacial constitutive law through the comparison of pull-out test data with numerical prediction. Figure **18** illustrates the superposition of the reference experimental force–slip curve and the corresponding optimized numerical response.

The model calibration was performed based on the parametric analysis described earlier. This sensitivity study enabled the identification of the key variables controlling the shape and features of the pull-out curve. Numerical optimization was therefore focused on the interfacial parameters shown to have the greatest influence:

- Interface stiffness modulus (H_f): Governs the initial elastic phase of the response.

- Maximum interfacial stress ($\tau_{\max}$): Defines the delamination criterion and the peak force.

- Fiber–matrix friction stress after decohesion (τ_d): Controls the residual strength plateau.

- Characteristic slip (s_k): Kinematic parameter that determines the softening slope during fiber extraction.

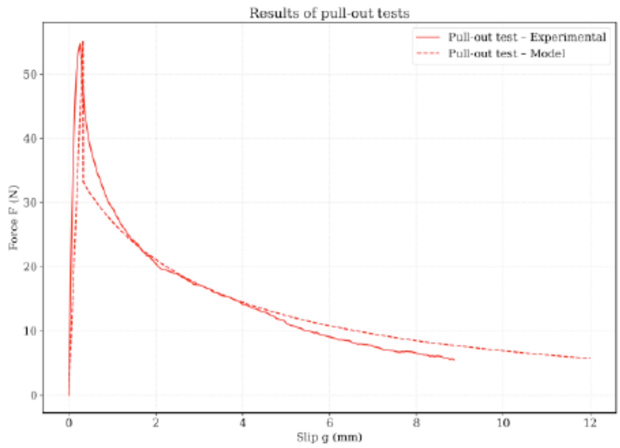

Figure 18: Comparison of numerical and experimental curves.

The correlation between the experimental and numerical curves demonstrates the capability of the model, particularly well-suited for short, straight fiber inclusions, to capture the complex behavior of the fiber–matrix interface. The pre-peak adhesion phase is accurately represented by the interfacial stiffness parameter H_f. The transition to peak, governed by the maximum interfacial stress $\tau_{\max}$, corresponds to the onset of interface degradation. The model translates this stage into an abrupt post-peak stress drop, characteristic of brittle chemical bond failure (total decohesion), before converging with the experimental softening branch.

The prolonged post-peak slip phase is dominated by interfacial friction, τ_d. It is important to note the significant influence of fiber embedment length: excessive anchorage, combined with high friction, can alter the shear stress distribution and potentially change the failure mode. Under such conditions, progressive interfacial slip may be replaced by tensile failure of the fiber itself during pull-out.

To complement the qualitative comparison between experimental and numerical pull-out curves, several quantitative indicators were introduced to evaluate the predictive capability of the model.

The relative error in peak pull-out force was computed as

$$Error_{F_{max}} = \frac{|F_{max}^{exp} - F_{max}^{num}|}{F_{max}^{exp}} \times 100 \quad (17)$$

The initial slope of the pull-out curve reflects the elastic response of the fiber–matrix system. The relative error in initial stiffness was calculated as

$$Error_{K} = \frac{|K^{exp} - K^{num}|}{K^{exp}} \times 100 \quad (18)$$

The pull-out energy, defined as the area under the force–displacement curve, represents the energy dissipated during fiber extraction and is a key indicator of toughness.

$$Error_{E} = \frac{|E^{exp} - E^{num}|}{E^{exp}} \times 100 \quad (19)$$

The overall agreement between numerical and experimental curves was evaluated using the Root Mean Square Error (RMSE):

$$RMSE = \sqrt{\frac{1}{n} \sum_{i=1}^{n} (F_i^{exp} - F_i^{num})^2} \quad (20)$$

The comparison between experimental and numerical pull-out responses demonstrates an overall satisfactory predictive capability of the proposed model. The peak pull-out force is reproduced with a very small relative error of approximately −1%, indicating that the calibrated interfacial shear strength accurately captures the onset of debonding and the maximum load transfer capacity of the fiber–earth interface. The pull-out energy shows a moderate deviation of about −15%, which remains acceptable given the inherent variability of natural fibers and the simplified representation of frictional sliding.

A larger discrepancy is observed for the initial stiffness, with an error of approximately 40%. This difference can be attributed to the simplified elastic assumptions adopted in the model, the difficulty of experimentally capturing the very early loading stage, and possible micro-slippage or seating effects during testing. Such deviations are commonly reported in pull-out modelling of natural fiber composites and mainly affect the initial portion of the response rather than the global load-bearing behavior.

The global agreement between experimental and numerical curves is confirmed by a RMSE of 3.5 N, which remains small compared to the maximum pull-out force. Overall, these results demonstrate that the model successfully reproduces the dominant mechanisms governing the pull-out process, particularly the peak load and the energy dissipation during fiber extraction.

4. CONCLUSIONS AND PERSPECTIVES

This study presented an integrated experimental–numerical investigation of the interface behavior between date palm fibers and unstabilized earth. Tensile tests, pull-out experiments, and analytical model were combined to characterize the mechanisms governing load transfer from adhesion to frictional sliding.

The results confirm that the fiber–earth interface plays a central role in the mechanical performance of bio-reinforced earthen materials. The calibrated numerical model successfully reproduces the main features of the pull-out response and provides a physically consistent description of adhesion, progressive debonding, and frictional sliding. The proposed methodology therefore establishes a micromechanical basis for predicting the crack-bridging capability and energy dissipation of palm fiber–reinforced earthen composites.

From a practical perspective, the findings highlight the importance of interfacial parameters, embedded length, and frictional resistance in controlling the toughness and ductility of earthen composites. The developed framework can support the performance-based design of sustainable fiber-reinforced earth construction materials and contributes to bridging the gap between experimental characterization and predictive modeling.

Despite these contributions, several limitations must be acknowledged. The model relies on simplified elastic assumptions and an equivalent diameter representation of the fiber geometry, while the natural variability of both fibers and earthen matrices introduces unavoidable scatter. In addition, environmental effects such as moisture variations, long-term durability, and cyclic loading were not considered.

Future work should therefore focus on incorporating hygro-mechanical effects, investigating fiber surface treatments, and extending the proposed approach to multi-fiber and structural-scale applications.

CONFLICT OF INTEREST STATEMENT

The authors declare that they have no conflicts of interest related to this work.

ACKNOWLEDGMENTS

The authors gratefully acknowledge Romain Gontero for providing the model developed in his thesis, which served as the foundation for this study. They also thank him for his insightful comments, explanations, and valuable assistance regarding modeling-related aspects.

AUTHOR CONTRIBUTIONS

F.A., B.A. and and F.F. conceived and designed the study. E.C-H., B.B. and A.D. performed the experiments and collected the data. E.C-H. conducted numerical simulations and formal analysis. E.C-H., B.B. and A.D. wrote the original draft, and all authors contributed to reviewing and editing the manuscript. F.A., B.A. and F.F. supervised the project and acquired funding.

REFERENCES

[1] Paulus J. Raw earth construction: qualitative, constructive, and architectural provisions - application to a practical case: Ouagadougou [master's thesis]. Liège (Belgium): University of Liège; 2015.

[2] Bailly GC, *et al*. Advancing earth-based construction: a comprehensive review of stabilization and reinforcement techniques for adobe and compressed earth blocks. Eng. 2024; 5(2): 750-783. https://doi.org/10.3390/eng5020041

[3] Phung TA. Formulation and characterization of an earth-plant fiber composite: cob [doctoral thesis]. Normandy (France): Normandy University; 2018.

[4] Eskandari A, *et al*. A laboratory study of tensile strength and tensile stress-strain relations of historical and new Persian adobes. Structures. 2025; 81: 110198. https://doi.org/10.1016/j.istruc.2025.110198

[5] Bertelsen IMG, *et al*. Influence of synthetic waste fibres on drying shrinkage cracking and mechanical properties of adobe materials. Constr Build Mater. 2021; 286: 122738. https://doi.org/10.1016/j.conbuildmat.2021.122738

[6] Pinto-Almeida C, *et al*. Experimental analysis of Ecuadorian adobe reinforced with natural fibers. Front Built Environ. 2025; 11: 1697128. https://doi.org/10.3389/fbuil.2025.1697128

[7] N'tsouaglo KH, *et al*. Influence of natural fiber properties on the mechanical performance of unfired earthen blocks. Int J Mater Sci Appl. 2025; 14(5): 200-211. https://doi.org/10.11648/j.ijmsa.20251405.13

[8] Koutous A, Hilali E. A review on the use of date palm fibers to reinforce earth-based construction materials. Mater Today Proc. 2023.

[9] Koutous A, Hilali E. Date palm fiber-reinforcement impact on rammed earth mechanical behavior. Constr Build Mater. 2025; 461: 139918. https://doi.org/10.1016/j.conbuildmat.2025.139918

[10] Aljewifi HAS, Edriss A, Mohamed A. Experimental study on addition of date palm fibers as reinforcement in gypsum mortar. Albahit J Appl Sci. 2021: 31-37.

[11] Laatar M, *et al*. Analyzing effects of different dosages of cement and date palm fiber lengths on the mechanical and thermal characteristics of compressed earth blocks. Jpn J Heat Mass Transfer. 2024; 37: 201-216. https://doi.org/10.17654/0973576324014

[12] Abdeldjebar R, *et al*. Effects of treated date palm fiber on durability of stabilized earth blocks (SEB). Int J Civ Eng Technol. 2018; 9(5): 293-305.

[13] Jacob PM, Thomas S, Varughese KT. A study of advances in characterization of interfaces and fiber surfaces in lignocellulosic fiber-reinforced composites. Compos Interfaces. 2005; 12(1-2): 95-124. https://doi.org/10.1163/1568554053542115

[14] Wang H, *et al*. Pull-out method for direct measuring the interfacial shear strength between short plant fibers and thermoplastic polymer composites. Holzforschung. 2014; 68(5). https://doi.org/10.1515/hf-2013-0052

[15] Oushabi A. The pull-out behavior of chemically treated lignocellulosic fibers/polymeric matrix interface (LF/PM): a review. Compos Part B Eng. 2019; 174: 107059. https://doi.org/10.1016/j.compositesb.2019.107059

[16] Mahi A, Fouchal F, Hamouine A, Abbes B. Interface behavior of composite stabilized earth blocks (SEB) - date palm fiber in earthen structures. Case study: Pull-out test (Experimentation & modeling). Eur J Environ Civ Eng. In press. 2025.

[17] Gontero R. Modeling the mechanical behavior of ultra-high performance fiber-reinforced concrete structures [doctoral thesis]. Toulouse (France): Université Paul Sabatier - Toulouse III; Québec (Canada): Université Laval; 2022.

[18] Sellier A. Anisotropic damage and visco-elasto-plasticity applied to multiphasic materials [research report]. Toulouse (France): LMDC - Laboratoire Matériaux et Durabilité des Constructions de Toulouse; Université de Toulouse III - Paul Sabatier; INSA de Toulouse; 2018.

[19] GOM GmbH. ARAMIS—user manual software, version 6.1 [software manual]. Braunschweig (Germany): GOM GmbH; 2009.

[20] Commissariat à l'énergie atomique et aux énergies alternatives (CEA). Cast3M finite element software [software]. France: CEA; Available from: https: //www-cast3m.cea.fr/

[21] Assia Z, Fouchal F, Hamouine A. Sustainability of stabilized earth blocks under chemical attack and environmental conditions. Constr Build Mater. 2019; 212: 787-798. https://doi.org/10.1016/j.conbuildmat.2019.03.324

[22] Walotek K, Bzówka J, Ciołczyk A. Examples of the Use of the ARAMIS 3D Measurement System for the Susceptibility to Deformation Tests for the Selected Mixtures of Coal Mining Wastes. Sensors. 2021; 21(13): 4600. https://doi.org/10.3390/s21134600

[23] Xu D, Cerbu C, Wang H, Rosca IC. Analysis of the hybrid composite materials reinforced with natural fibers considering digital image correlation (DIC) measurements. Mech Mater. 2019; 13: 46-56. https://doi.org/10.1016/j.mechmat.2019.05.001

[24] Nammur G, Naaman AE, Clark SK. Analytical prediction of the pull-out behavior of steel fibers in cementitious matrices. MRS Online Proc Libr. 1987; 114: 217-224. https://doi.org/10.1557/PROC-114-217

[25] Zhan MY. Multilevel modeling of fiber-reinforced concrete and application to numerical simulations of tunnel lining segments [PhD thesis]. Bochum (Germany): Ruhr University Bochum; 2016.

[26] Zhan Y, Meschke G. Analytical model for the pullout behavior of straight and hooked-end steel fibers. J Eng Mech. 2014; 140(12): 04014091. https://doi.org/10.1061/(ASCE)EM.1943-7889.0000800

[27] Rajagopala K, Parameswaran VS. A study on the mechanics of fiber debonding in concrete with micro-reinforcement. Mater Struct. 1975; 8(46): 305-314. https://doi.org/10.1007/BF02478855

[28] Ávila F, Fagone M, Gallego R, *et al*. Experimental and numerical evaluation of the compressive and shear behavior of unstabilized rammed earth. Mater Struct. 2023; 56: 118. https://doi.org/10.1617/s11527-023-02206-9

[29] Zheng Z, Su H, Wang W, *et al*. A new hydro-mechanical coupling constitutive model for brittle rocks considering initial compaction, hardening and softening behaviors under complex stress states. Geomech Geophys Geo-energ Geo-resour. 2023; 9: 68. https://doi.org/10.1007/s40948-023-00607-2

https://doi.org/10.12974/2311-8717.2026.14.04